Deliverable Report

Deliverable No: D2.3

Deliverable Title: Hybrid polarization- OAM entanglement

Grant Agreement number: 255914

Project acronym: PHORBITECH

Project title: A Toolbox for Photon Orbital Angular Momentum Technology

Project website address: www.phorbitech.eu

Name, title and organisation of the scientific representative of deliverable's lead beneficiary (task leader):

Dr. Fabio Sciarrino

Sapienza Università di Roma

Rome, Italy

Deliverable table

Deliverable no.	D2.3
Deliverable name	Hybrid polarization-OAM entanglement
WP no.	2
Lead beneficiary no.	2 (UROM)
Nature	R
Dissemination level	PU
Delivery date from Annex I	Month 12
Actual delivery date	30 September 2011

D2.3) Hybrid polarization-OAM entanglement: Generation of hybrid OAM-polarization entangled photon pairs by starting with polarization-entangled pairs generated by SPDC and applying spin-to-orbital conversion to one arm. [Excerpt from GA-Annex I DoW]

Hybrid entangled states exhibit entanglement between different degrees of freedom of a particle pair and thus could be useful for asymmetric optical quantum network where the communication channels are characterized by different properties.

In Reference [1] UNAP and UGLAS have reported quantum states of single photons and of correlated photon pairs exhibiting "hybrid" entanglement between spin and orbital angular momentum. These states are obtained from entangled photon pairs emitted by spontaneous parametric down conversion by employing a q plate for coupling the spin and orbital degrees of freedom of a photon. Entanglement and contextual quantum behavior (that is also nonlocal, in the case of photon pairs) has been demonstrated by the reported violation of the Clauser-Horne-Shimony-Holt inequality. In addition, a classical analog of the hybrid spin-orbit photonic entanglement is reported and discussed.

In Reference [2] UROM has reported the first experimental realization of hybrid polarization-orbital angular momentum (OAM) entangled states by adopting a spontaneous parametric down conversion source of polarization entangled states and a polarization-OAM transferrer. The generated quantum states have been characterized through quantum state tomography. Finally, the violation of Bell's inequalities with the hybrid two photon system has been observed.

In Reference [3] UROM and UNAP have exploited hybrid entangled states to investigate the resilience of OAM. In order to characterize the degradation undergone by the information content of qubits encoded in a bidimensional subspace of the orbital angular momentum degree of freedom of photons, UROM and UNAP investigated how the state fidelity is affected by a transverse obstruction placed along the propagation direction of the light beam. Emphasis is placed on the effects of planar and radial hard-edged aperture functions on the state fidelity of Laguerre-Gaussian transverse modes and the entanglement properties of polarization-OAM hybrid-entangled photon pairs.

Publications:
[1] "Spin-orbit hybrid entanglement of photons and quantum contextuality"
E. Karimi, J. Leach, S. Slussarenko, B. Piccirillo, L. Marrucci, L. Chen, W. She, S. Franke-Arnold, M. J. Padgett, E. Santamato, Phys. Rev. A 82, 022115 (2010)
[2] "Generation of hybrid polarization-orbital angular momentum entangled states"
E. Nagali, F. Sciarrino, Opt. Express 18, 18243-18248 (2010).
[3] "Resilience of orbital-angular-momentum photonic qubits and effects on hybrid entanglement"
D. Giovannini, E. Nagali, L. Marrucci, F. Sciarrino, Phys. Rev. A 83, 042338 (2011).

Spin-orbit hybrid entanglement of photons and quantum contextuality

Ebrahim Karimi,[1,*] Jonathan Leach,[2] Sergei Slussarenko,[1] Bruno Piccirillo,[1,3] Lorenzo Marrucci,[1,4] Lixiang Chen,[5] Weilong She,[5] Sonja Franke-Arnold,[2] Miles J. Padgett,[2] and Enrico Santamato[1,3]

[1]*Dipartimento di Scienze Fisiche, Università di Napoli "Federico II," Compl. Univ. di Monte S. Angelo, I-80126 Napoli, Italy*

[2]*Department of Physics and Astronomy, University of Glasgow, Glasgow, Scotland G12 8QQ, United Kingdom*

[3]*Consorzio Nazionale Interuniversitario per le Scienze Fisiche della Materia, Napoli*

[4]*CNR-SPIN, Compl. Univ. di Monte S. Angelo, I-80126 Napoli, Italy*

[5]*State Key Laboratory of Optoelectronic Materials and Technologies, Sun Yat-sen University, Guangzhou 510275, China*

(Received 6 May 2010; published 26 August 2010)

We demonstrate electromagnetic quantum states of single photons and of correlated photon pairs exhibiting "hybrid" entanglement between spin and orbital angular momentum. These states are obtained from entangled photon pairs emitted by spontaneous parametric down conversion by employing a q plate for coupling the spin and orbital degrees of freedom of a photon. Entanglement and contextual quantum behavior (that is also nonlocal, in the case of photon pairs) is demonstrated by the reported violation of the Clauser-Horne-Shimony-Holt inequality. In addition, a classical analog of the hybrid spin-orbit photonic entanglement is reported and discussed.

DOI: 10.1103/PhysRevA.82.022115 PACS number(s): 03.65.Ud, 03.65.Ta, 03.67.Bg, 42.50.Xa

I. INTRODUCTION

Entangled states are at the heart of most quantum paradoxes and provide the main tool for quantum information processing, including applications such as teleportation, cryptography, superdense coding, and so on. Entangled quantum states are also the basis of Bell's inequality violations, which ruled out classical hidden-variable theories in favor of quantum mechanics [1]. Bell's inequalities were originally derived for two particles, as a consequence of locality and realism. In almost all experimental demonstrations of these inequalities to date, the same degree of freedom of two particles has been used, e.g., the spin of a photon. Very recently, however, the case of so-called hybrid entanglement, occurring when the involved degrees of freedom of the two particles are not the same, has attracted a certain interest, and the first experimental demonstrations with spin and spatial-mode degrees of freedom have been reported [2–4]. Using different degrees of freedom also opens up another opportunity, i.e., that of realizing entanglement between different degrees of freedom of a single particle. In this case, no role is played by nonlocality, but Bell-type inequalities can still be formulated by assuming realism and the so-called non-contextuality of the two involved commuting observables, i.e., the assumption that the result of a particular measurement of one observable is determined independently of any simultaneous measurement of the other one [5–7]. Noncontextual hidden variable models have been excluded by recent experiments where the violation of suitable inequalities was observed using neutrons [8], ions [9], and single photons prepared in entangled spin-path states [10]. Finally, single-particle entanglement, in the case of bosons such as photons, has a classical analog that is obtained by replacing single-photon states with multiphoton coherent states realized within the same field mode [11]. Such a classical analog helps visualizing the nature of the single-particle entanglement.

A particularly convenient framework in which to explore these concepts is provided by photons carrying both spin angular momentum (SAM) and orbital angular momentum (OAM). While the former is the most widely employed internal degree of freedom of photons for quantum manipulations, the latter is becoming an interesting additional resource for quantum applications (see, e.g., Refs. [12–15]). In this work, we study three conceptually related experimental situations. First, heralded single photons are prepared in a state where SAM and OAM are entangled (as proposed in Refs. [16,17]) and are then used for testing the contextuality of different degrees of freedom of the same particle. Second, correlated photon pairs, where the SAM of one photon is entangled with the OAM of the other, i.e., photon pairs exhibiting SAM-OAM hybrid entanglement, are generated and used for testing the contextuality and nonlocality of these degrees of freedom when they are spatially separated. Finally, optical coherent states involving many photons are used to demonstrate a classical analog of SAM-OAM hybrid entanglement.

II. EXPERIMENTAL SETUP

The experimental layout we used in the quantum regime (the first two experiments) is presented in Fig. 1. Our down-conversion source generates photon pairs that are entangled in the OAM degree of freedom [18,19], each photon being horizontally polarized, as described by

$$|\psi\rangle = \sum_{m=-\infty}^{\infty} c_{|m|}|m\rangle_o^A|-m\rangle_o^B|H\rangle_\pi^A|H\rangle_\pi^B. \quad (1)$$

Here A and B denote the signal and idler photons traveling along the two corresponding arms of the setup shown in Fig. 1 and π, o denote SAM and OAM degrees of freedom, respectively. The integer m is the photon OAM in units of $\hbar$ and H denotes horizontal linear polarization.

A. Single-photon experiment

In this case we use photon B to herald a single photon A which we convert into an OAM-SAM maximally entangled state. Starting from state $|\psi\rangle$ given in Eq. (1), we

*karimi@na.infn.it

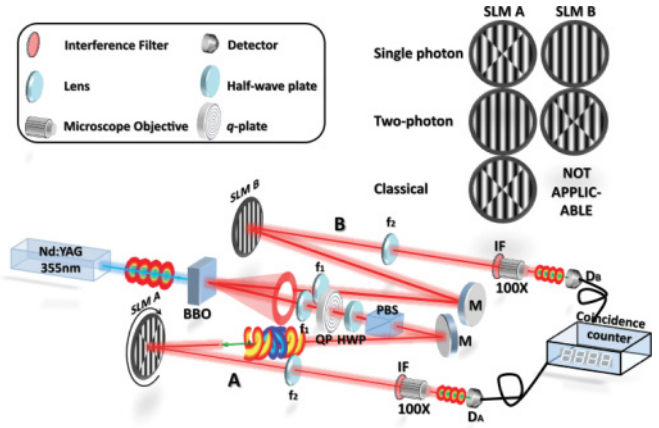

FIG. 1. (Color online) Setup used for the two quantum-regime experiments. A Nd:YAG laser with average power of 150 mW at 355 nm pumps a nonlinear crystal of β-barium borate (BBO) cut for degenerate type I noncollinear phase matching which emits OAM-entangled H-polarized photon pairs at 710 nm (see Ref. [19] for details). The photons of each pair are split in arms A and B, respectively. Legend of the main components (see also graphic symbol legend in the upper left inset): f_1, f_2, lenses for beam control; QP, q plate; HWP, half-wave plate; PBS, polarizer; M, mirror; SLM A and SLM B, spatial light modulators; IF, interference filter for bandwidth definition; 100×, microscope objectives for fiber coupling; D_A, D_B, photon detectors. In the classical-regime experiment, the optical line is the same as arm A. (Top-right inset) Computer-generated hologram patterns displayed on the two SLMs in the three experiments.

postselect photon pairs having $m = 0$, i.e., in state $|\psi\rangle = c_0|0\rangle_o^A|0\rangle_o^B|H\rangle_\pi^A|H\rangle_\pi^B$, by coupling photon B into a single-mode optical fiber. Photon A is thus also projected into $m = 0$. Spatial light modulator SLM B in this case is patterned as a uniform grating, deflecting the beam but not affecting its transverse spatial mode (see the upper right inset of Fig. 1). Photon A is sent first through a q plate [20,21] to generate the maximally entangled SAM-OAM state [22]

$$|\Phi^+\rangle^A = \frac{1}{\sqrt{2}}\left(|R\rangle_\pi^A|{+2}\rangle_o^A + |L\rangle_\pi^A|{-2}\rangle_o^A\right), \qquad (2)$$

where L and R denote left-circular and right-circular polarization states, respectively. The polarization state of photon A emerging from the q plate is then measured by a half-wave plate (HWP) oriented at a variable angle $\theta/2$ and a fixed linear polarizer, restoring the horizontal polarization. This HWP-polarizer combination filters incoming photons having linear polarization at angle θ with respect to the horizontal direction. In the circular polarization basis, the state of the filtered photons is written as $|\theta\rangle_\pi = \frac{1}{\sqrt{2}}(e^{i\theta}|L\rangle_\pi + e^{-i\theta}|R\rangle_\pi)$. The SAM measurement does not affect the OAM degree of freedom. Noncontextuality can be assumed between the z component of photon SAM and OAM, because, in the paraxial approximation, the SAM operator $\widehat{S}_z$ commutes with the OAM operator $\widehat{L}_z$. After SAM filtering, the photon's OAM is also measured by a suitable computer-generated hologram, displayed on SLM A, followed by coupling into a single-mode fiber. The hologram pattern is defined by the four-sector alternated π-shift phase structure shown in the upper-right inset of Fig. 1, with the four sectors rotated at a variable angle χ (the grating fringes are not rotated). On diffraction, this hologram transforms the photons arriving in the OAM superposition state $|\chi\rangle_o = \frac{1}{\sqrt{2}}(e^{2i\chi}|{+2}\rangle_o + e^{-2i\chi}|{-2}\rangle_o)$ back into the $m = 0$ state, which is then filtered by coupling in fiber. The OAM superposition state $|\chi\rangle_o$ is the spatial mode analog of the linear polarization, and we may refer to its angle χ as to its "orientation" [23]. The overall effect of our apparatus is therefore to perform a joint measurement of the polarization and spatial mode orientations of A photons at angles θ and χ, respectively. When photon A is in the entangled Bell state described by Eq. (2), we expect that the final probability to detect it (in coincidence with the B trigger photon) is given by

$$P(\theta,\chi) = \left|{}^A\langle\Phi^+| \cdot |\theta\rangle_\pi^A|\chi\rangle_o^A\right|^2 \propto \cos^2(\theta - 2\chi). \qquad (3)$$

To test entanglement we adopt the Clauser-Horne-Shimony-Holt (CHSH) inequality, given by [24]

$$S = |E(\theta,\chi) - E(\theta,\chi') + E(\theta',\chi) + E(\theta',\chi')| \leqslant 2, \quad (4)$$

where $E(\theta,\chi)$ is calculated from the A-B photon coincidence counts $C(\theta,\chi)$ according to

$$E(\theta,\chi) = \frac{C(\theta,\chi) + C\left(\theta+\frac{\pi}{2},\chi+\frac{\pi}{4}\right) - C\left(\theta+\frac{\pi}{2},\chi\right) - C\left(\theta,\chi+\frac{\pi}{4}\right)}{C(\theta,\chi) + C\left(\theta+\frac{\pi}{2},\chi+\frac{\pi}{4}\right) + C\left(\theta+\frac{\pi}{2},\chi\right) + C\left(\theta,\chi+\frac{\pi}{4}\right)}. \qquad (5)$$

While the CHSH inequality is commonly applied to nonlocal measurements on two spatially separated entangled photons, testing for hidden variable theories, here we apply it to single-photon entanglement to test for contextuality. In Fig. 2(a)

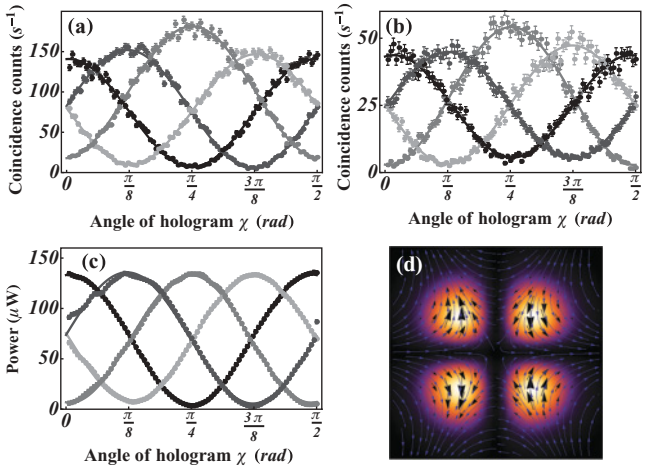

FIG. 2. (Color online) The experimental coincidence counts as a function of orientation of the sector hologram for different values of polarization direction, for (a) heralded single photons, (b) photon pairs, and (c) coherent-states. Black dots respresent $\theta = 0$, dark gray dots $\theta = \pi/4$, gray dots $\theta = 2\pi/4$, and light gray dots $\theta = 3\pi/4$. The solid lines are the best theoretical fit over the experimental data. The fringe contrast is about 90%, which is much larger than 70.7%, as required for Bell's inequality verification. (d) Simulated intensity and polarization distribution patterns of the optical field for the beam emerging from the q plate in the case of horizontal polarization input beam.

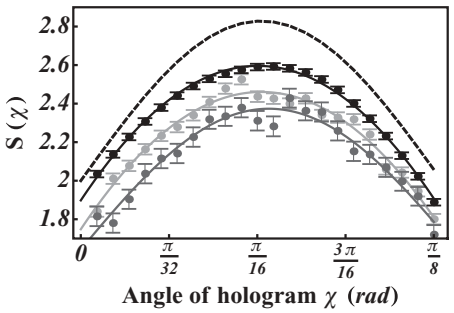

FIG. 3. The CHSH S value in a region where it is larger than the classical limit 2. The choice of the variables appearing in Eq. (4) is the following: $\theta = 0, \theta' = \pi/4$, χ is the plot abscissa, $\chi' = \chi + \pi/8$. The light gray, gray, and black dots correspond to the experimental data in the case of single-photon (a), photon-pairs (b), and classical-wave (c) SAM-OAM experiments, respectively. The dashed line is the quantum mechanical ideal prediction. In the two cases (a) and (b), at $\chi = \pi/16$, the CHSH inequality is violated respectively by 17 and 10 standard deviations. The classical case (c) is plotted for comparison

the coincidence counts are shown as a function of spatial mode orientation χ for different values of polarization angles θ. The occurrence of high-visibility fringes indicates (single-particle) entanglement in the SAM-OAM spaces. The CHSH S value calculated from these data is shown in Fig. 3 (gray dots). A violation of the CHSH inequality is clearly obtained, in good agreement with quantum theory predictions, confirming the entanglement and providing a demonstration of quantum SAM-OAM contextuality for single photons.

B. Two-photon experiment

In this case, we generate and verify entanglement between the SAM of one photon and the OAM of the other, i.e., we demonstrate nonlocal hybrid entanglement in these two degrees of freedom. To this purpose, the four-sector and uniform holograms of arms **A** and **B** were swapped, as displayed in the upper right inset of Fig. 1. The q plate in arm **A** and the sector hologram in arm **B** of the apparatus, together with subsequent coupling into the single-mode fiber before detection, act to postselect the photons with $m = \pm 2$ in Eq. (1), i.e., the postselected initial two-photon state is $|\psi\rangle = \frac{1}{\sqrt{2}} c_2 (|2\rangle_o^A |-2\rangle_o^B + |-2\rangle_o^A |2\rangle_o^B) |H\rangle_\pi^A |H\rangle_\pi^B$. The photon A passes through the q plate, acting in this case as a OAM-to-SAM transferrer [22], so the OAM eigenstates $m = \pm 2$ are mapped into L and R polarized photons with $m = 0$, respectively. After this process, the photon pair is projected into the nonlocal state

$$|\phi\rangle_{nl} = \frac{1}{\sqrt{2}} \left(|L\rangle_\pi^A |+2\rangle_o^B + |R\rangle_\pi^A |-2\rangle_o^B \right) |0\rangle_o^A |H\rangle_\pi^B, \quad (6)$$

where the SAM of one photon is maximally entangled with the OAM of the other. Next, the polarization of the A photon is measured by the HWP rotated at angle $\theta/2$ followed by the polarizer, and the spatial mode of the B photon by the sector hologram rotated at angle χ followed by coupling in fiber. Well-defined coincidence fringes with visibility up to 90% are obtained, as shown in Fig. 2(b). Repeating the measurements for different angles θ and χ, the quantity S was evaluated from Eqs. (4) and (5) and the violation of the CHSH inequality was verified, as shown in Fig. 3 (light gray dots). This violation provides a demonstration of SAM-OAM hybrid entanglement and nonlocality for separated photon pairs.

C. Classical light experiment

In our final experiment, we move to a classical regime of nonseparable optical modes occupied by many photons, corresponding to coherent quantum states. A 100-mW frequency-doubled linearly polarized continuous wave Nd:YVO_4 laser beam is sent in an optical line equal to arm A of our quantum apparatus to obtain, after the q plate, a coherent state in the SAM-OAM nonseparable mode $|\Phi^+\rangle$ given by Eq. (2) [26]. The calculated structure of this mode is shown in Fig. 2(d) for a given input polarization. The mode nonseparability is evident, as the polarization is spatially nonuniform [17]. The beam polarization is then filtered by the combination of the HWP at angle θ and polarizer and its spatial mode by the sector hologram rotated at angle χ, as in the single-photon experiment (Fig. 1). In this case, no trigger is used and the count rates $C(\theta, \chi)$ in Eq. (5) are replaced by average power measurements, corresponding to photon fluxes. When the angles θ and χ are changed, high-contrast sinusoidal fringes proportional to $\cos^2(\theta - 2\chi)$ were observed in the overall transmitted power fraction, as shown in Fig. 2(c). As shown in Fig. 3 (black dots) we note that the classical experiment mimics the results of the single-photon experiment. However, the experiment can of course also be interpreted without assuming the existence of photons. In this case, SAM and OAM measurements can be understood just as wave filtering procedures, and no conclusion can be drawn about discrepancies between classical-realistic and quantum behavior. Nevertheless, providing a classical analog of single-particle entanglement is interesting in itself and may offer the basis for some entirely classical implementations of quantum computational tasks [27].

III. CONCLUSIONS

In conclusion, we have demonstrated hybrid entanglement between the spin and the orbital angular momentum of light in two different regimes: single photons and entangled photon pairs. We have reported an additional classical experiment which mimics the quantum result and although the experimental results appear very similar in the three cases, they provide different and complementary insight into the contextual quantum nature of light.

ACKNOWLEDGMENT

The project PHORBITECH acknowledges the financial support of the Future and Emerging Technologies (FET) programme within the Seventh Framework Programme for Research of the European Commission, under FET-Open grant number 255914.

[1] J. S. Bell, Rev. Mod. Phys. **38**, 447 (1966).
[2] X. S. Ma, A. Qarry, J. Kofler, T. Jennewein, and A. Zeilinger, Phys. Rev. A **79**, 042101 (2009).
[3] L. Neves, G. Lima, A. Delgado, and C. Saavedra, Phys. Rev. A **80**, 042322 (2009).
[4] F. Bussieres, J. A. Slater, J. Jin, N. Godbout, and W. Tittel, Phys. Rev. A **81**, 052106 (2010).
[5] S. M. Roy and V. Singh, Phys. Rev. A **48**, 3379 (1993).
[6] N. D. Mermin, Rev. Mod. Phys. **65**, 803 (1993).
[7] B. H. Liu, Y. F. Huang, Y. X. Gong, F. W. Sun, Y. S. Zhang, C. F. Li, and G. C. Guo, Phys. Rev. A **80**, 044101 (2009).
[8] Y. Hasegawa *et al.*, Nature (London) **425**, 45 (2003).
[9] G. Kirchmair *et al.*, Nature (London) **460**, 494 (2009).
[10] B. R. Gadway, E. Galvez, and F. DeZela, J. Phys. B **42**, 015503 (2009).
[11] R. J. C. Spreeuw, Found. Phys. **28**, 361 (1998).
[12] G. Molina-Terriza, J. P. Torres, and L. Torner, Nat. Phys. **3**, 305 (2007).
[13] S. Franke-Arnold, L. Allen, and M. Padgett, Laser & Photon. Rev. **2**, 299 (2008).
[14] J. T. Barreiro, T.-C. Wei, and P. G. Kwiat, Nat. Phys. **4**, 282 (2008).
[15] E. Nagali *et al.*, Nat. Photon. **3**, 720 (2009).
[16] L. Chen and W. She, J. Opt. Soc. Am. B **27**, A7 (2009).
[17] C. V. S. Borges, M. Hor-Meyll, J. A. O. Huguenin, and A. Z. Khoury, e-print arXiv:0911.2440v1.
[18] B. Jack *et al.*, New J. Phys. **11**, 103024 (2009).
[19] J. Leach *et al.*, Opt. Express **17**, 8287 (2009).
[20] L. Marrucci, C. Manzo, and D. Paparo, Phys. Rev. Lett. **96**, 163905 (2006).
[21] L. Marrucci, C. Manzo, and D. Paparo, Appl. Phys. Lett. **88**, 221102 (2006).
[22] E. Nagali, F. Sciarrino, F. DeMartini, L. Marrucci, B. Piccirillo, E. Karimi, and E. Santamato, Phys. Rev. Lett. **103**, 013601 (2009).
[23] This spatial state corresponds to a hypergeometric-Gaussian mode [25] having the same azimuthal profile as a Hermite-Gauss mode (1, 1) rotated at angle χ with respect to the horizontal plane.
[24] J. F. Clauser, M. A. Horne, A. Shimony, and R. A. Holt, Phys. Rev. Lett. **23**, 880 (1969).
[25] E. Karimi *et al.*, Opt. Lett. **32**, 3053 (2007).
[26] We note that, when the classical states are described as coherent quantum states, the state of the nonseparable mode $|\alpha_{\Phi^+}\rangle$ is found to be decomposable in the direct product of the coherent states of the two SAM-OAM eigenmodes $|\frac{1}{\sqrt{2}}\alpha_{(R,2)}\rangle$ and $|\frac{1}{\sqrt{2}}\alpha_{(L,-2)}\rangle$ so no SAM-OAM photon entanglement is actually present in the beam [17].
[27] R. J. C. Spreeuw, Phys. Rev. A **63**, 062302 (2001).

Generation of hybrid polarization-orbital angular momentum entangled states

Eleonora Nagali[1] **and Fabio Sciarrino**[1,2,*]

[1]*Dipartimento di Fisica, Sapienza Università di Roma, Roma 00185, Italy*
[2]*Istituto Nazionale di Ottica (INO-CNR), L.go E. Fermi 6, Florence 50125, Italy*
**fabio.sciarrino@uniroma1.it*

Abstract: Hybrid entangled states exhibit entanglement between different degrees of freedom of a particle pair and thus could be useful for asymmetric optical quantum network where the communication channels are characterized by different properties. We report the first experimental realization of hybrid polarization-orbital angular momentum (OAM) entangled states by adopting a spontaneous parametric down conversion source of polarization entangled states and a polarization-OAM transferrer. The generated quantum states have been characterized through quantum state tomography. Finally, the violation of Bell's inequalities with the hybrid two photon system has been observed.

OCIS codes: (270.0270) Quantum Optics; (270.5585) Quantum information and processing.

References and links

1. N. Gisin, G. Ribordy, W. Tittel, and H. Zbinden, "Quantum cryptography," Rev. Mod. Phys. **74**, 145 (2002).
2. F. De Martini, and F. Sciarrino, "Non-linear parametric processes in quantum information," Prog. Quantum Electron. **29**, 165 (2005).
3. P. G. Kwiat, K. Mattle, H. Weinfurter, and A. Zeilinger, "New High-Intensity Source of Polarization-Entangled Photon Pairs," Phys. Rev. Lett. **75**, 4337 (1995).
4. P. G. Kwiat, E. Waks, A. G. White, I. Appelbaum, and P. H. Eberhard, "Ultrabright source of polarization-entangled photons," Phys. Rev. A **60**, R773 (1999).
5. C. Cinelli, G. Di Nepi, F. De Martini, M. Barbieri, and P. Mataloni, "Parametric source of two-photon states with a tunable degree of entanglement and mixing: Experimental preparation of Werner states and maximally entangled mixed states," Phys. Rev. A **70**, 022321 (2004).
6. G. Molina-Terriza, J. P. Torres, and L. Torner, "Twisted photons," Nat. Phys. **3**, 305 (2007).
7. S. Franke-Arnold, L. Allen, and M. Padgett, "Advances in optical angular momentum," Laser Photon. Rev. **4**, 299313 (2008).
8. J. T. Barreiro, T. C. Wei, and P. G. Kwiat, "Beating the channel capacity limit for linear photonic superdense coding," Nature Phys. **4**, 282 (2008).
9. E. Nagali, L. Sansoni, F. Sciarrino, F. De Martini, L. Marrucci, B. Piccirillo, E. Karimi, and E. Santamato, "Optimal quantum cloning of orbital angular momentum photon qubits via Hong-Ou-Mandel coalescence," Nat. Photon. **3**, 720 (2009).
10. A. Mair, A. Vaziri, G. Weihs, and A. Zeilinger, "Entanglement of the orbital angular momentum states of photons," Nature (London) **412**, 313 (2001).
11. A. Vaziri, J. W. Pan, T. Jennewein, G. Weihs, and A. Zeilinger, "Concentration of Higher Dimensional Entanglement: Qutrits of Photon Orbital Angular Momentum," Phys. Rev. Lett. **91**, 227902 (2003).
12. J. P. Torres, Y. Deyanova, and L. Torner, "Preparation of engineered two-photon entangled states for multidimensional quantum information," Phys. Rev. A **67**, 052313 (2003).
13. G. Molina-Terriza, A. Vaziri1, J. Rehcek, Z. Hradil, and A. Zeilinger, "Triggered Qutrits for Quantum Communication Protocols," Phys. Rev. Lett. **92**, 167903 (2004).

#128118 - $15.00 USD Received 6 May 2010; revised 14 Jul 2010; accepted 18 Jul 2010; published 10 Aug 2010

14. N. K. Langford, R. B. Dalton, M. D. Harvey, J. L. O'Brien, G. J. Pryde, A. Gilchrist, S. D. Bartlett, and A. G. White, "Measuring Entangled Qutrits and Their Use for Quantum Bit Commitment," Phys. Rev. Lett. **93**, 053601 (2004).
15. G. Molina-Terriza, A. Vaziri, R. Ursin, and A. Zeilinger, "Experimental Quantum Coin Tossing," Phys. Rev. Lett. **94**, 040501 (2005).
16. J. T. Barreiro, N. K. Langford, N. A. Peters, and P.G. Kwiat, "Generation of Hyperentangled photons pairs," Phys. Rev. Lett. **95**, 260501 (2005).
17. S. S. R. Oemrawsingh, X. Ma, D. Voigt, A. Aiello, E. R. Elie, G. W. Hooft, and J. P. Woerdman, "Experimental Demonstration of Fractional Orbital Angular Momentum Entanglement of Two Photons," Phys. Rev. Lett. **95**, 240501 (2005).
18. B. P. Lanyon, T. J. Weinhold, N. K. Langford, J. L. OBrien, K. J. Resch, A. Gilchrist, and A. G. White, "Manipulating Biphotonic Qutrits," Phys. Rev. Lett. **100**, 060504 (2008).
19. X. Ma, A. Qarry, J.s Kofler, T.Jennewein, and A. Zeilinger, "Experimental violation of a Bell inequality with two different degrees of freedom of entangled particle pairs," Phys. Rev. A **79**, 042101 (2009).
20. L. Neves, G. Lima, A. Delgado, and C. Saavedra, "Hybrid photonic entanglement: Realization, characterization, and applications," Phys. Rev. A **80**, 042322 (2009).
21. L. Chen and W. She, "Teleportation of a controllable orbital angular momentum generator," Phys. Rev. A **80**, 063831 (2009).
22. E. Nagali, F. Sciarrino, F. De Martini, L. Marrucci, B. Piccirillo, E. Karimi, and E. Santamato, "Quantum information transfer from spin to orbital angular momentum of photons," Phys. Rev. Lett. **103**, 013601 (2009).
23. E. Nagali, F. Sciarrino, F. De Martini, L. Marrucci, B. Piccirillo, E. Karimi, and E. Santamato, "Polarization control of single photon quantum orbital angular momentum states," Opt. Express **17**, 18745 (2009).
24. L. Marrucci, C. Manzo, and D. Paparo, "Optical Spin-to-Orbital Angular Momentum Conversion in Inhomogeneous Anisotropic Media," Phys. Rev. Lett. **96**, 163905 (2006).
25. D. F. V. James, P. G. Kwiat, W. J. Munro, and A. G. White, "Measurement of qubits," Phys. Rev. A **64**, 052312 (2001).
26. J. F. Clauser, M. A. Horne, A. Shimony, and R. A. Holt, "Proposed Experiment to Test Local Hidden-Variable Theories," Phys. Rev. Lett. **23**, 880 (1969).

1. Introduction

The development of tailored photonic sources suitable to produce entanglement represents a crucial resource for quantum information applications like quantum communication schemes, quantum cryptographic protocols, and for fundamental tests of quantum theory [1]. Parametric down conversion has been proven to be the best source of entangled photon pairs so far in an ever increasing number of experiments on the foundations of quantum mechanics and in the new field of quantum communication [2]. Optical implementation of quantum information processing have been realized by several, different approaches, each one with its own advantages and limitations concerning the generation, manipulation, transmission, detection, robustness of the information carriers. While initially most of the effort has been devoted to the implementation of polarization entangled states [3–5], in the last few years entangling different degrees of freedom has attracted much attention. Within this scenario, the orbital angular momentum (OAM), the degree of freedom of light associated with rotationally structured transverse spatial modes, has been recently exploited to encode quantum states [6–9]. Generation of OAM-entangled pairs of photons has been demonstrated mainly by spontaneous parametric down-conversion [10–18]. By merging different techniques, it is possible to exploit the power and the advantages of each method and hence overcome the present technological limitations.

Hybrid entangled states exhibit entanglement between different degrees of freedom of a particle pair. The generation of such states can be useful for asymmetric optical quantum network where the different communication channels adopted for transmitting quantum information exhibit different properties. In such a way one could adopt the suitable degree of freedom with larger robustness along the channel. From a fundamental point of view, the observation of nonlocality with hybrid systems proves the fundamental independence of entanglement from the physical realization of the adopted Hilbert space. Very recently the hybrid entanglement of photon pairs between the path (linear momentum) of one photon and the polarization of the other

#128118 - $15.00 USD Received 6 May 2010; revised 14 Jul 2010; accepted 18 Jul 2010; published 10 Aug 2010

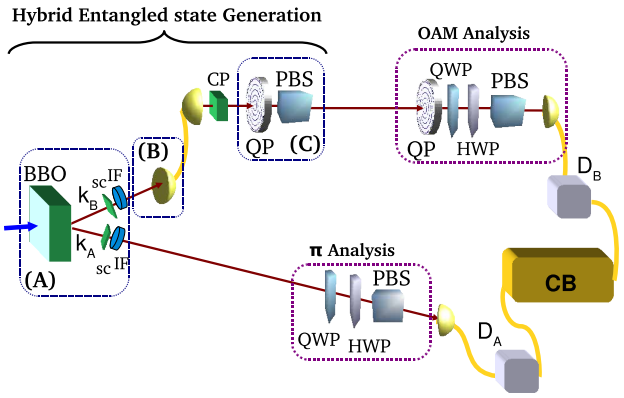

Fig. 1. Experimental setup adopted for the generation and characterization of hybrid π-OAM entangled states.**(A)**Generation of polarization entangled photons on modes k_A and k_B.**(B)**Projection on the OAM state with $m = 0$ through the coupling on a single mode fiber (SMF).**(C)**Encoding of the state in the OAM subspace o_2 through the $\pi \rightarrow o_2$ transferrer.

photon has been reported by two different techniques [19,20]. Nevertheless, the capability of generating hybrid-entangled state encoded in the polarization and OAM of single photons could be advantageous since it could allow the engineering of qubit-qudit entangled states, related to the different Hilbert space dimensionality of the two degrees of freedom. It has been pointed out that such states are desiderable for quantum information and communication protocols, as quantum teleportation, and for the possibility to send quantum information through an optical quantum network composed by optical fiber channels and free-space [20,21].

In this paper, we report the experimental realization of hybrid polarization-OAM entangled states, by adopting the deterministic polarization-OAM transferrer introduced in Ref. [22,23]. Polarization entangled photon pairs are created by spontaneous parametric down conversion, the spatial profile of the twin photons is filtered through single mode fibers and finally the polarization is coherently transferred to OAM state for one photon. A complete characterization of the hybrid entangled quantum states has been carried out by adopting the quantum state tomography technique. This result, together with the achieved generation rate, the easiness of alignment and the high quality of the generated state, can make this optical source a powerful tool for advanced quantum information tasks. For instance the OAM features can be more appropriate for mapping single photon states in atomic systems.

2. Experimental apparaturs and generation of hybrid states

Let us now describe the experimental layout shown in Fig. 1. A 1.5mm thick β-barium borate crystal (BBO) cut for type-II phase matching [3], is pumped by the second harmonic of a Ti:Sa mode-locked laser beam, and generates via spontaneous parametric fluorescence polarization entangled photon pairs on modes k_A and k_B with wavelength $\lambda = 795$ nm, and pulse bandwidth $\Delta\lambda = 4.5$ nm, as determined by two interference filters (IF). The spatial and temporal walk-off is compensated by inserting a $\frac{\lambda}{2}$ waveplate and a 0.75 mm thick BBO crystal (SC) on each output mode k_A and k_B [3]. Thus the source generates photon pair in the singlet entangled state encoded in the polarization, i.e. $\frac{1}{\sqrt{2}}(|H\rangle^A|V\rangle^B - |V\rangle^A|H\rangle^B)$. The photon generated on mode k_A is sent through a standard polarization analysis setup and then coupled to a single mode fiber

#128118 - $15.00 USD Received 6 May 2010; revised 14 Jul 2010; accepted 18 Jul 2010; published 10 Aug 2010

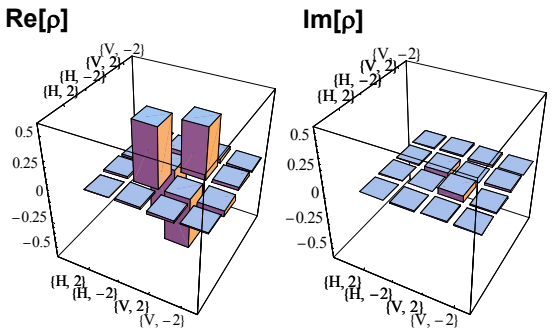

Fig. 2. Experimental density matrix of the hybrid entangled state generated after the transferrer transformation on photons on k_B mode. Each measurement setting lasted 15s.

connected to the single-photon counter modules (SPCM) D_A. The photon generated on mode k_B is coupled to a single mode fiber, in order to collapse its transverse spatial mode into a pure TEM_{00}, corresponding to OAM $m = 0$. After the fiber output, two waveplates compensate (CP) the polarization rotation introduced by the fiber. To transform the polarization entangled pairs into an hybrid entangled state the photon B is sent through the quantum transferrer $\pi \rightarrow o_2$, which transfers the polarization quantum states in the OAM degree of freedom.

The quantum transferrers have been extensively described in [22,23]. To sum up, the transformation $|\varphi\rangle_\pi|0\rangle_o \rightarrow |H\rangle_\pi|\varphi\rangle_{o_2}$ carried out by the transferrer, is achieved through a q-plate device, which couples the spinorial (polarization) and orbital contributions of the angular momentum of photons [22,24]. Here and after, we will denote the bidimensional OAM subspace with $m = \pm 2$, where m denotes here the OAM per photon along the beam axis in units of $\hbar$, as $o_2 = \{|+2\rangle, |-2\rangle\}$. According to the nomenclature $|\varphi\rangle_\pi|\phi\rangle_{o_2}$, the $|\cdot\rangle_\pi$ and $|\cdot\rangle_{o_2}$ stand for the photon quantum state 'kets' in the polarization and OAM degrees of freedom. Following the same convention, the OAM equivalent of the two basis linear polarizations $|H\rangle$ and $|V\rangle$ are then defined as $|h\rangle = (2^{-1/2})(|+2\rangle + |-2\rangle); |v\rangle = (2^{-1/2})(|+2\rangle - |-2\rangle)$. Finally, the $\pm 45^\circ$ angle "anti-diagonal" and "diagonal" linear polarizations will be hereafter denoted with the kets $|+\rangle = (2^{-1/2})(|H\rangle + |V\rangle)$ and $|-\rangle = (2^{-1/2})(|H\rangle - |V\rangle)$, and the corresponding OAM states are defined analogously: $|a\rangle = e^{-i\pi/4}(|+2\rangle + i|-2\rangle)(2^{-1/2}); |d\rangle = e^{i\pi/4}(|+2\rangle - i|-2\rangle)(2^{-1/2})$. The transformation established by a q-plate with $q = 1$, as the one adopted in our experiment, can be described as:

$$\begin{aligned} |L\rangle_\pi|0\rangle_o &\overset{QP}{\rightarrow} |R\rangle_\pi|+2\rangle_{o_2} \\ |R\rangle_\pi|0\rangle_o &\overset{QP}{\rightarrow} |L\rangle_\pi|-2\rangle_{o_2} \end{aligned} \tag{1}$$

where L and R denote the left and right circular polarization states, respectively. Any coherent superposition of the two input states given in Eq. (1) is preserved by the QP transformation, leading to the equivalent superposition of the corresponding output states [22]. Thus by combining the transformation induced by the q-plate and a polarizing beamsplitter the map $|\varphi\rangle_\pi|0\rangle_o \rightarrow |H\rangle_\pi|\varphi\rangle_{o_2}$ can be achieved with an efficiency of conversion equal to 50%. It is possible to realize a fully *deterministic* transferrer $\pi \rightarrow o_2$ at the price of a more complex optical layout, based on a q-plate and a Mach-Zehnder interferometer, as shown in [23]. After the transferrer operation the polarization entangled state is transformed into the hybrid entangled state:

$$\frac{1}{\sqrt{2}}(|H\rangle^A_\pi|+2\rangle^B_{o_2} - |V\rangle^A_\pi|-2\rangle^B_{o_2})|0\rangle^A_o|H\rangle^B_\pi \tag{2}$$

#128118 - $15.00 USD Received 6 May 2010; revised 14 Jul 2010; accepted 18 Jul 2010; published 10 Aug 2010

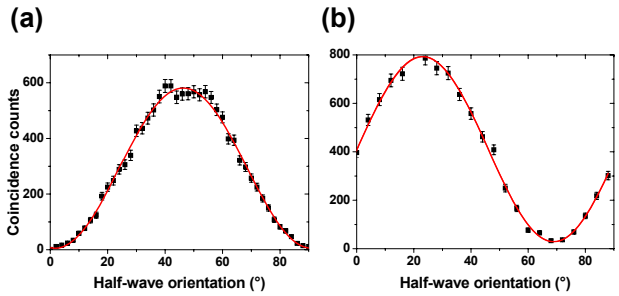

Fig. 3. Coincidence rate $[D_A, D_B]$ measured as a function of the angle θ of the half wave plate on the arm k_A for OAM detected state **(a)** $|+2\rangle$ and **(b)** $|h\rangle_{o_2}$.

In order to analyze with high efficiency the OAM degree of freedom, we exploited the $o_2 \rightarrow \pi$ transferrer, as shown in [9, 23]. By this approach any measurement on the OAM state is achieved by measuring the polarization after the transferrer device, as shown in Fig. 1. Finally the photon has been coupled to a single mode fiber and then detected by D_B connected to the coincidence box (CB), which records the coincidence counts between $[D_A, D_B]$. We observed a final coincidence rate equal to $C = 100 coinc/s$ within a coincidence window of 3 ns. This experimental data is in agreement with the expected value, determined from $C_{source} = 6kHz$ after taking into account two main loss factors: hybrid state preparation probability p_{prep}, and detection probability p_{det}. p_{prep} depends on the conversion efficiency of the q-plate (0.80 ± 0.05) and on the probabilistic efficiency of the quantum transferrer $\pi \rightarrow o_2$ (0.5), thus leading to $p_{prep} = 0.40 \pm 0.03$. The detection efficiency includes the q-plate conversion efficiency (0.8), the transferrer $o_2 \rightarrow \pi$ (0.5), and the single mode fiber coupling (0.2). Hence $p_{det} = 0.08$. The observed experimental rate includes a reduction factor ~ 8 due to the adoption of probabilistic transferrers [23], and by achieving a higher single mode fiber coupling efficiency. Hence, by modifying the transferrers, we expect to achieve a detection rate equal to about $800 coinc/s$.

3. Characterization of the state

To completely characterize the state in Eq. 2 we reconstructed the density matrix of the quantum state. The tomography reconstruction requires the estimation of 16 operators [25] through 36 separable measurements on the polarization-OAM subspaces. We carried out the reconstruction of the density matrix $\rho^{A,B}_{\pi,o_2}$ after the polarization-OAM conversion. The experimental results are reported in Fig. 2, with the elements of the density matrices expressed in the polarization and OAM basis $\{|H,+2\rangle, |H,-2\rangle, |V,+2\rangle, |V,-2\rangle\}$. The fidelity with the singlet states $|\Psi^-\rangle$ has been evaluated to be $F(|\Psi^-\rangle, \rho^{A,B}_{\pi,o_2}) = (0.957 \pm 0.009)$, while the experimental linear entropy of the state reads $S_L = (0.012 \pm 0.002)$. A more quantitative parameter associated to the generated polarization-entangled states is given by the concurrence $C = (0.957 \pm 0.002)$. These values demonstrate the high degree of hybrid entanglement generation.

To further characterize the hybrid quantum states, the violation of Bell's inequalities with the two photon system have been addressed. First, we measured the photon coincidence rate as a function of the orientation of the half-wave plate on Alice arm for two different OAM basis analysis, namely $\{|+2\rangle_{o_2}, |-2\rangle_{o_2}\}$ and $\{|h\rangle_{o_2}, |v\rangle_{o_2}\}$. The variation of the number of coincidences $N(\theta)$ with the angle θ is in agreement with the one expected for entangled states such as $N(\theta) = N_0(1 + cos\theta)$: Fig. 3. The coincidence fringe visibility reaches the values $V = (0.966 \pm 0.001)$ and $V = (0.930 \pm 0.007)$. Hence, a non-locality test, the CHSH one [26], has been carried out. Each of two partners, A (Alice) and B (Bob) measures a dichotomic

#128118 - $15.00 USD Received 6 May 2010; revised 14 Jul 2010; accepted 18 Jul 2010; published 10 Aug 2010

observable among two possible ones, i.e. Alice randomly measures either **a** or **a'** while Bob measures **b** or **b'**, where the outcomes of each measurement are either $+1$ or -1. For any couple of measured observables $(A = \{\mathbf{a},\mathbf{a'}\}, B = \{\mathbf{b},\mathbf{b'}\})$, we define the following correlation function $E(A,B) = \frac{N(+,+)+N(-,-)-N(+,-)-N(-,+)}{N(+,+)+N(-,-)+N(+,-)+N(-,+)}$ where $N(i,j)$ stands for the number of events in which the observables A and B have been found equal to the dichotomic outcomes i and j. Finally we define the parameter S which takes into account the correlations for the different observables

$$S = E(\mathbf{a},\mathbf{b}) + E(\mathbf{a'},\mathbf{b}) + E(\mathbf{a},\mathbf{b'}) - E(\mathbf{a'},\mathbf{b'}) \tag{3}$$

Assuming a local realistic theory, the relation $|S| \leq S_{CHSH} = 2$ holds. To carry out a non-locality test in the hybrid regime, we define the two sets of dichotomic observables for A and B. For Alice the basis **a** and **a'** correspond, respectively, to the linear polarization basis $\{|H\rangle_\pi, |V\rangle_\pi\}$ and $\{|+\rangle_\pi, |-\rangle_\pi\}$. For Bob the basis **b** and **b'** correspond, respectively, to the OAM basis $\{cos(\frac{\pi}{8})|+2\rangle - sin(\frac{\pi}{8})|-2\rangle, -sin(\frac{\pi}{8})|+2\rangle + cos(\frac{\pi}{8})|-2\rangle\}$ and $\{cos(\frac{\pi}{8})|+2\rangle + sin(\frac{\pi}{8})|-2\rangle, sin(\frac{\pi}{8})|+2\rangle - cos(\frac{\pi}{8})|-2\rangle\}$. Experimentally we obtained the following value by carrying out a measurement with a duration of $60s$ and an average statistics per setting equal to about 1500 events: $S = (2.51 \pm 0.02)$. Hence a violation by more than 25 standard deviation over the value $S_{CHSH} = 2$ is obtained. This experimental value is in good agreement with an experimental visibility of $V = (0.930 \pm 0.007)$ which should lead to $S = (2.57 \pm 0.02)$.

4. Conclusion

In conclusion, we presented a source of polarization-OAM hybrid entanglement based on SPDC source and $\pi \rightarrow o_2$ transferrer. We have shown that this system provides quantum states with high fidelity and with a bright generation rate. Moreover by adopting several concatenated q-plates the generation of hybrid states with higher OAM value could be obtained. Hybrid entangled states could be adopted to carry out quantum state teleportation between different degrees of freedom of light. Furthermore by inserting a quantum transferrer $\pi \rightarrow o_2$ also on mode k_A, a controllable source of OAM entangled states could be achieved.

Acknowledgement

This work was supported by FARI project, Finanziamento Ateneo 2009 of Sapienza Universitá di Roma, project PHORBITECH of the Future and Emerging Technologies (FET) programme within the Seventh Framework Programme for Research of the European Commission, under FET-Open grant number 255914, and project HYTEQ FIRB-Futuro in Ricerca (MIUR).

#128118 - $15.00 USD Received 6 May 2010; revised 14 Jul 2010; accepted 18 Jul 2010; published 10 Aug 2010

Resilience of orbital-angular-momentum photonic qubits and effects on hybrid entanglement

Daniele Giovannini,[1] Eleonora Nagali,[1] Lorenzo Marrucci,[2,3] and Fabio Sciarrino[1,4,*]

[1]*Dipartimento di Fisica, Sapienza Università di Roma, Roma I-00185, Italy*

[2]*Dipartimento di Scienze Fisiche, Università di Napoli Federico II, Complesso Universitario di Monte S. Angelo, I-80126 Napoli, Italy*

[3]*CNR-SPIN, Complesso Universitario di Monte S. Angelo, I-80126 Napoli, Italy*

[4]*Istituto Nazionale di Ottica (INO-CNR), Largo E. Fermi 6, Florence I-50125, Italy*

(Received 17 November 2010; published 29 April 2011)

The orbital angular momentum of light (OAM) provides a promising approach for the implementation of multidimensional states (qudits) for quantum-information purposes. In order to characterize the degradation undergone by the information content of qubits encoded in a bidimensional subspace of the orbital angular momentum degree of freedom of photons, we study how the state fidelity is affected by a transverse obstruction placed along the propagation direction of the light beam. Emphasis is placed on the effects of planar and radial hard-edged aperture functions on the state fidelity of Laguerre-Gaussian transverse modes and the entanglement properties of polarization-OAM hybrid-entangled photon pairs.

DOI: 10.1103/PhysRevA.83.042338 PACS number(s): 03.67.−a, 42.50.Ex, 42.50.Dv

I. INTRODUCTION

In quantum-information theory the fundamental unit of information is a two-level quantum system, the qubit. As in classical information science with bits, all quantum-information tasks can at least in theory be performed through just qubits and quantum gates operating on qubits [1–3]. For quantum-information purposes and the effective production and processing of robust qubits, as well as that of multidimensional quantum states or qudits [4,5], considerable interest has been recently focused on the generation and manipulation of helical laser beams. These optical waves, which have been shown to carry well-defined values of orbital angular momentum (OAM), are well described in terms of Laguerre-Gaussian (LG) modes, containing an ℓ-charged optical phase singularity (or optical vortex) at their beam axis [6–8]. Any two of such OAM modes with opposite values of ℓ and a common radial profile, here denoted as $|+\ell\rangle$ and $|-\ell\rangle$, define a basis of a bidimensional OAM subspace, $o_{|\ell|}$, in which one can encode a generic qubit. These specific OAM subspaces are particularly convenient to this purpose as they are not affected by propagation-induced decoherence, because the radial profile factorizes and can be usually ignored [9]. Experimentally, single-photon qubits in the OAM subspace o_2 can be efficiently encoded and readout by means of "polarization-OAM transferrers" [10,11], which are devices based on a recently introduced optical element called the "q-plate" [12].

The growing number of works demonstrating simple quantum-information protocols based on OAM-encoded qubits raise questions about how practical such an approach is, as compared, for instance, with the standard polarization encoding. For example, one can ask how sensitive are these OAM-encoded qubits to small optical misalignments or other nonideality of typical setups. More in general, studies of the resilience of OAM-encoded qubits or qudits in free-space propagation under the effect of perturbations and of imperfect detection are pivotal for the use of the OAM of light for quantum communication tasks. Previous works on LG modes in the classical regime showed, for example, the spread of measured transverse modes when planar restrictions spanning an angular range of less than 2π are placed along the beam [13,14], the consequences of noncoaxial mode detection [15], and the effect of turbulence on OAM-encoded information [16–21].

The purpose of this paper is to characterize the degradation undergone by the information encoded in o_2 OAM qubits when transverse hard-edged optical apertures are placed along the propagation direction of the beam, both in the classical and quantum regimes. The apertures considered in this work have one of the two shapes shown in Fig. 1, which are here taken to mimic the typical effect of optical misalignments or of the finite numerical aperture of optical components.

This paper is organized as follows: Section II introduces a classical theoretical model, based on the functional shape of LG modes, used to assess the degradation undergone by states belonging to three different o_2 bases as a consequence of the perturbation introduced during propagation by the two kinds of optical apertures. In Sec. III, we compare the theoretical predictions with the results of experiments performed in the classical regime. In Sec. IV, we finally present the experimental results concerning the effects of the previously introduced obstructions on the entanglement properties of a hybrid polarization-OAM entangled pair of twin photons [22,23], that is, a pair of entangled photons whose entanglement is encoded in two different degrees of freedom.

II. THEORY

An OAM eigenstate, $|\ell\rangle$, is here taken to denote a pure LG mode, corresponding to the wave function $A(x,y,z) = A(r,\phi,z) = A_0(r,z)\,e^{i\ell\phi}$ with azimuthal index ℓ, where z is the propagation axis; x,y are the Cartesian coordinates for the transverse plane; and r,ϕ are the corresponding polar coordinates. LG modes are characterized also by another index, p, determining the radial profile. In the following, except where explicitly stated otherwise, this radial index is understood to be $p = 0$ and is omitted.

*fabio.sciarrino@uniroma1.it

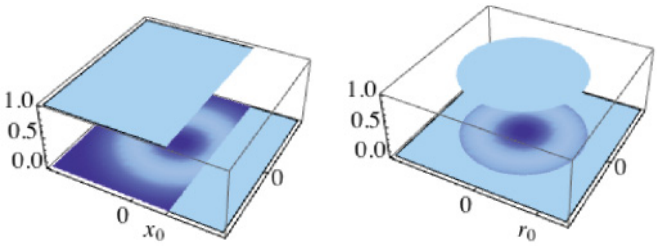

(a) $B(x_0, x; y)$ (b) $\Pi(r_0, r; \phi)$

FIG. 1. (Color online) Aperture functions: (a) planar transverse obstruction $B(x_0,x; y)$ (knife), and (b) radial obstruction $\Pi(r_0,r; \phi)$ (iris).

Generic OAM qubits are described by superpositions $|\psi\rangle = \alpha|+2\rangle + \beta|-2\rangle$, where α and β are complex coefficients. We consider, in particular, the following six representative states, belonging to three mutually unbiased bases of the OAM subspace o_2: $|l\rangle = |+2\rangle$, $|r\rangle = |-2\rangle$; $|h\rangle = (|l\rangle + |r\rangle)/\sqrt{2}$, $|v\rangle = -i(|l\rangle - |r\rangle)/\sqrt{2}$; and $|d\rangle = (1-i)(|l\rangle + i|r\rangle)/2$, $|a\rangle = (1+i)(|l\rangle - i|r\rangle)/2$ [24]. The wave functions $A(x,y,z)$ of these states are given by the corresponding superpositions of pure LG modes. All input wave functions are normalized for integration in any given (arbitrary) transverse plane z of the beam, i.e., $\int\int |A|^2 dx\, dy = 1$.

As mentioned in the Introduction, we consider two sets of optical apertures: (i) a half-plane obstruction with its edge located at the variable abscissa x_0, described by the transmittance function $B(x_0,x; y) = \theta(x_0 - x)$, where $\theta(x)$ is the Heaviside step function [see Fig. 1(a)]; and (ii) an iris with variable aperture radius r_0, described by the transmittance function $\Pi(r_0,r; \phi) = \theta(r_0 - r)$ [see Fig. 1(b)]. The first kind of aperture is meant to mimic the perturbations arising from small transverse optical misalignments, while the second corresponds to introducing optical elements having a small numerical aperture.

Now, given an arbitrary input qubit, $|\psi\rangle$, as described by the wave function A, the perturbed state $|\psi'\rangle$ obtained immediately after the aperture is given by the (not normalized) wave function $A' = AB$ or $A' = A\Pi$, respectively [see, e.g., Figs. 2(a) and 2(b)]. Given the normalization of the input wave function, the transmitted fraction of photons after the aperture is given by $T = \int\int |A'|^2 dx\, dy$. We then introduce the following two projections:

$$\kappa_\psi = \int_{-\infty}^{\infty} dx \int_{-\infty}^{\infty} dy\; A^*(x,y)\; A'(x,y) \tag{1a}$$

$$\kappa_{\psi^\perp} = \int_{-\infty}^{\infty} dx \int_{-\infty}^{\infty} dy [A^\perp(x,y)]^* A'(x,y), \tag{1b}$$

where $A^\perp$ is the wave function of the orthogonal state within the o_2 OAM subspace (with $p = 0$). We take the final detection probability of states ψ and $\psi^\perp$ to be given by $P(\psi) = |\kappa_\psi|^2$ and $P(\psi^\perp) = |\kappa_{\psi^\perp}|^2$, respectively. Therefore, $P_{o_2} = |\kappa_\psi|^2 + |\kappa_{\psi^\perp}|^2$ represents the probability of information preservation in the OAM subspace o_2 (with $p = 0$) after the initial mode has been transmitted through the aperture. The complementary fraction $1 - P_{o_2}$ of photons is lost either because they are absorbed in the aperture (as given by the fraction $1 - T$) or because they are transferred out of the $o_2 p = 0$ subspace and therefore are finally filtered out by the measurement process (note that this implies that the detection optics is assumed to have a small numerical aperture, thus strongly favoring $p = 0$ over higher radial modes). The computed OAM spectrum broadening induced by the planar aperture (function B) is shown in Fig. 3, for different positions of the aperture as specified by the resulting transmittance T.

The detected photons, however, will transport a partially degraded OAM qubit. The amount of quantum-information content that can be reconstructed by a receiver by means of projective measurements can be described through a fidelity parameter F defined as $F = P(\psi)/[P(\psi) + P(\psi^\perp)]$.

For each OAM state $|\psi\rangle$ and each position x_0 (or radius r_0) of the obstruction, the probabilities $P(\psi)$ and $P(\psi^\perp)$ were computed using numerical integration. The corresponding predictions for the information-preservation probability P_{o_2} are shown in Fig. 4, together with the corresponding mode profiles.

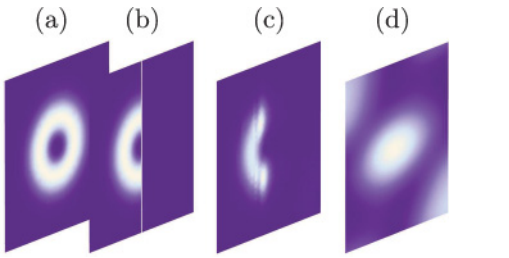

FIG. 2. (Color online) Propagation of an $LG_{0,+2}$ beam (basis state $|l\rangle$) through a $B(x_0)$ aperture function with $T = 0.5$. Profiles are drawn to the same scale. From left to right: (a) unperturbed transverse intensity profile; (b) intensity profile immediately after the aperture function (0.01 nm from the obstruction); (c) calculated profile after free-space propagation of the perturbed mode for $d = 30$ cm after the obstruction; (d) calculated profile after the insertion of a q-plate optical element (see Ref. [12]), used for the conversion into a TEM_{00} mode after the propagation of $d = 30$ cm.

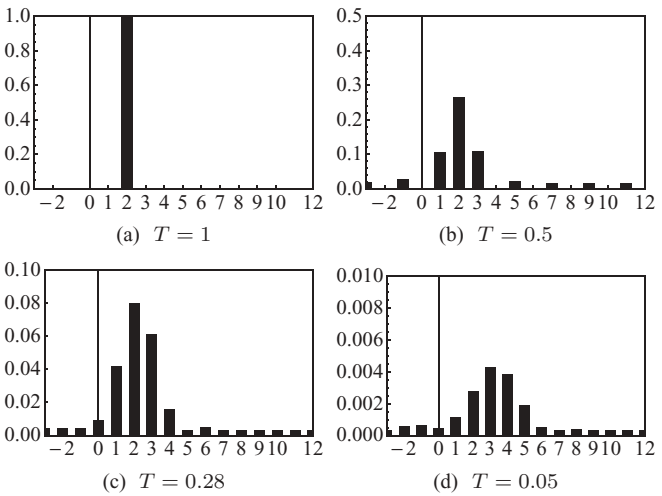

FIG. 3. (Color online) Spread in the measurement probabilities of OAM modes with $\ell' = -2, \ldots, 12$ for various positions x_0 of a $B(x_0)$ aperture inserted into the path of an $\ell = 2$ beam (i.e., for decreasing values of transmittance T).

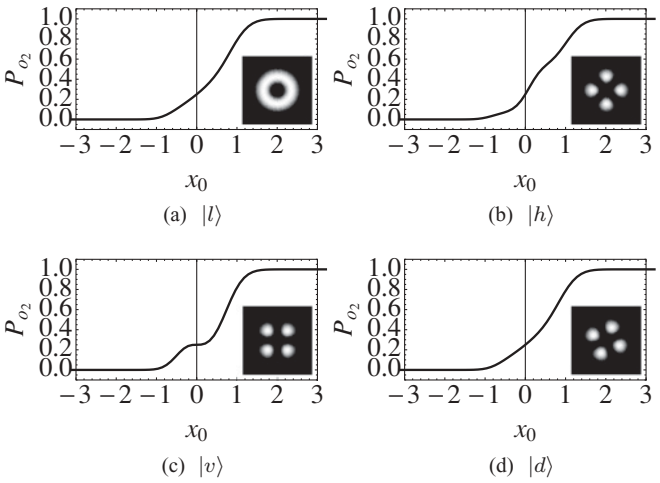

FIG. 4. (Color online) Theoretical curves of P_{o_2} for aperture function $B(x_0)$ for input states $|l\rangle$ ($|r\rangle$ exhibits the same curve), $|h\rangle$, $|v\rangle$, and $|d\rangle$ (or $|a\rangle$). The aperture edge position x_0 is given in units of the beam waist w_0). The mode intensity profile of each state is also shown in the inset of each panel. The aperture edge is vertically oriented in the inset frames.

The computed mean-information-preservation probability P_{o_2} and fidelity F for the aperture function $B(x_0)$, averaged over the six OAM states, are shown in Fig. 5 as solid lines. The mean P_{o_2} relative to the aperture function $P(r_0)$ is shown in Fig. 6. The theoretical fidelity in this second case is constantly unitary, because the rotational symmetry is not broken by the aperture.

III. CLASSICAL EXPERIMENTS

Classical measurements were performed on coherent beams by generating the OAM modes in o_2 corresponding to the six

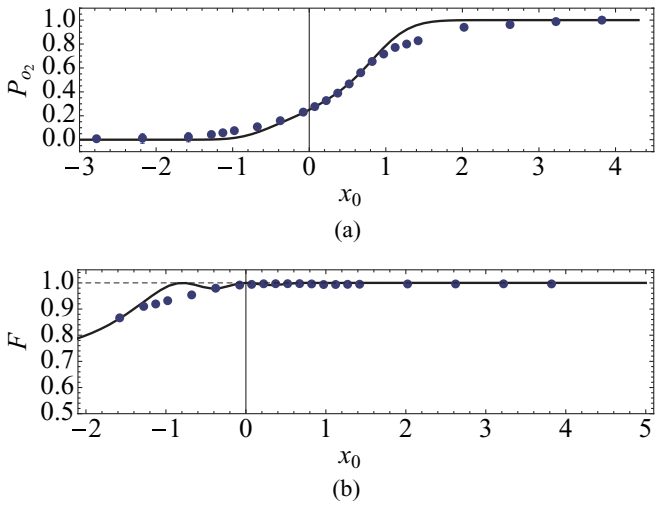

FIG. 5. (Color online) Average information-preservation probability P_{o_2} (a) and fidelity (b) for planar aperture function $B(x_0)$: lines are theoretical predictions, circles are data obtained in classical measurements (average over states $|d\rangle$ and $|a\rangle$), and experimental errors are negligible. The aperture edge position x_0 is given in units of the beam waist w_0).

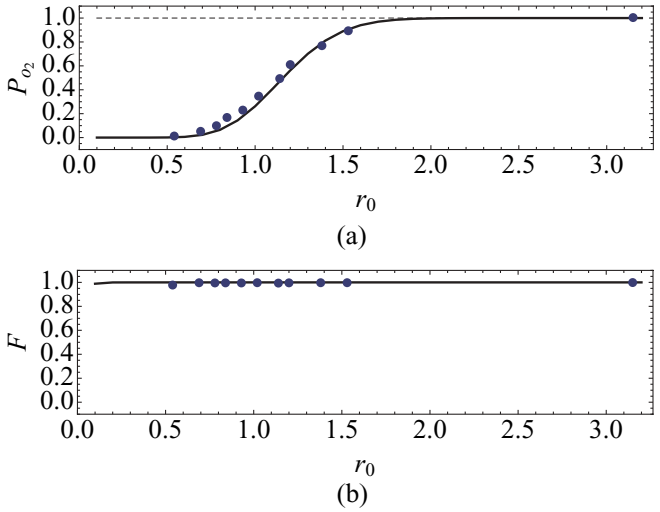

FIG. 6. (Color online) Average information-preservation probability P_{o_2} (a) and fidelity (b) for circular aperture function $\Pi(r_0)$: lines are theoretical predictions, and circles are data obtained in classical measurements, as a function of the aperture radius r_0 in units of the beam waist w_0.

states ($|l\rangle$, $|r\rangle$), ($|h\rangle$, $|v\rangle$, $|d\rangle$, $|a\rangle$) and then placing either a knife (aperture function B) or an iris (function Π) along the beam path. The perturbed modes $|\psi'\rangle$ were then projected onto $|\psi\rangle$ and $|\psi^{\perp}\rangle$ by the analysis setup. We assumed that no significant degradation (except possibly for some additional small losses) occurs to the quantum information in the analysis setup.

In the experimental implementation, a continuous laser beam was coupled to a single-mode fiber in order to collapse its transverse spatial mode into a pure TEM_{00}, corresponding to OAM $\ell = 0$. After the fiber, a polarization set was used to prepare the input polarization state as one of the six qubits. The beam was then sent through a quantum transferrer, $\pi \rightarrow o_2$, which transferred the polarization quantum state to the OAM degree of freedom, thus obtaining one of the input OAM state to be studied [9,10]. In order to analyze with high efficiency the OAM state after the aperture, we then exploited an inverse $o_2 \rightarrow \pi$ transferrer and a polarization analysis set [9]. The inverse transferrer includes the coupling to a single-mode fiber, which in our case was achieved with a typical efficiency $\eta = 14.8\%$. Although the q-plate device used in the transferrers is known to generate a radial profile more complex than a pure LG mode [25], only the $p = 0$ radial modes will be efficiently coupled to the final single-mode fiber used in our analysis setup, so that the $p = 0$ assumption used in our theory appears to be well justified.

The experimental average data for aperture B and states $|d\rangle$ and $|a\rangle$ are shown in Fig. 5, and those for Π and all o_2 basis states are shown in Fig. 6.

A comparison between the theoretical curves and the experimental points in Figs. 5, 6, and 7 shows a good quantitative agreement. Indeed, as highlighted in Fig. 7, even when the position of the obstruction causes a significant decrease of the transmittance, the state fidelity remains always above 90%. This demonstrates that, even in a high-loss regime, the initial information content encoded in the unperturbed state is preserved in the given OAM subspace even if a significant

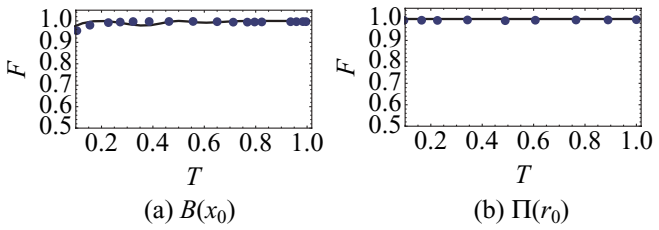

FIG. 7. (Color online) Fidelities versus transmittance in the classical regime for the two aperture geometries: theoretical predictions (solid lines) and experimental data (circles).

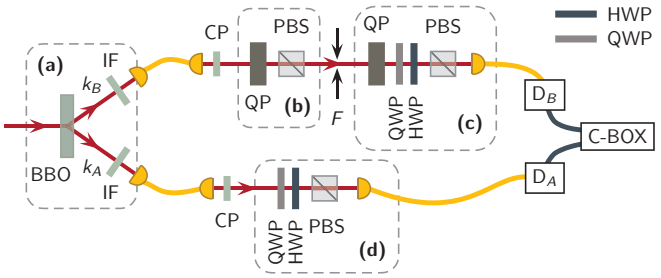

FIG. 8. (Color online) Experimental setup for the generation of hybrid polarization-OAM entangled photon pairs, with the application of the aperture function F. (a) Generation of polarization-entangled photons on modes k_A and k_B. (b) Encoding of the state of one photon in the OAM subspace o_2 through the $\pi \rightarrow o_2$ transferrer. (c) OAM analysis. (d) Polarization analysis.

spread of the initial OAM spectrum takes place (see Fig. 3). Any discrepancies may be explained by an imperfect mode generation and, more appreciably, by a higher sensitivity to small fluctuations of the fidelity parameter when T approaches zero. This result shows that the information content of OAM qubits exhibits a remarkable resilience to perturbations such as those examined here.

In particular, the reported high fidelities correspond to the experimental fact that after the aperture one still has $|\kappa_{\psi^\perp}|^2 \ll |\kappa_\psi|^2$. This result is tied to the moderate spread of the OAM spectrum of the perturbed state even for low values of T and the progressive shift of the central spectral state when the initial mode is almost completely blocked, as shown in Fig. 3.

The present work focuses on qubits encoded in the bidimensional o_2 subspace. However, it is worth noting that higher-order subspaces o_k, with LG basis states $\{|+k\rangle, |-k\rangle\}$, are likely to offer higher and higher resilience, the higher the OAM winding number k (while we may expect a lower resilience in the o_1 subspace). Indeed, as shown in Fig. 3 for the $|\ell| = 2$ case, the increased distance $\Delta\ell$ between the two orthogonal basis states causes the spread of the detection probabilities around a perturbed basis state $|+k\rangle$ to have a decreasing overlap with $|-k\rangle$ as k increases. Therefore, while the information-preservation probability is strongly affected, the fidelity is expected to remain high even for very low transmittance. Of course, these results do not apply to other subspaces of OAM not involving opposite values of the OAM eigenvalue, so it remains to be seen whether the same resilience can be achieved for OAM qudits. Our results are also in qualitative agreement with former investigations on the OAM spectrum broadening occurring for LG beams passing through variable angular optical apertures [26,27].

IV. RESILIENCE OF HYBRID POLARIZATION-OAM ENTANGLEMENT

After the classical regime experiments, we moved to a quantum regime. We are specifically interested in evaluating the resilience of the entanglement involving the OAM degree of freedom of a photon, under the effect of an optical aperture. In particular, we have considered the case of a planar aperture [function $B(x_0)$] inserted in the path of a photon belonging to photon pair that is initially prepared in a hybrid-entangled state of OAM and polarization. The choice of using hybrid entanglement is mainly practical, as we start from a polarization-entangled pair of photons and then the quantum state of one of the two photons is transferred into the OAM by using a polarization-OAM transferrer, as recently reported in [22].

Polarization-entangled photon pairs were created by spontaneous parametric down-conversion; the spatial profile of the twin photons was filtered through single-mode fibers, and the polarization state of one of them was coherently transferred to the corresponding OAM state. The aperture was then used to perturb the photon carrying the OAM entangled information and, finally, the two-photon quantum state was analyzed and the fidelity with the initially prepared state was computed. The experimental arrangement, shown in Fig. 8, is analogous to that adopted in the high-quality generation of hybrid polarization-OAM entangled photon pairs in [22], and it extends to the case of entangled photon pairs in the setup used in the previous section. A 1.5-mm-thick β-barium borate crystal (BBO) cut for type-II phase matching was pumped by the second harmonic of a Ti:sapphire mode-locked laser beam. Via spontaneous parametric fluorescence, the BBO generated polarization-entangled photon pairs on modes k_A and k_B with wavelength $\lambda = 795$ nm and pulse bandwidth $\Delta\lambda = 4.5$ nm, as determined by two interference filters (IF). The spatial and temporal walk-off was compensated by inserting a $\lambda/2$ wave plate and a 0.75-mm-thick BBO crystal on each output mode k_A and k_B [28]. The source thus generated photon pairs in the polarization-encoded singlet entangled state, i.e., $\frac{1}{\sqrt{2}}(|H\rangle_A|V\rangle_B - |V\rangle_A|H\rangle_B)$.

The photon in mode k_A was sent through a standard polarization analysis setup and then coupled to a single-mode fiber connected to the single-photon counter modules D_A. The photon in mode k_B was coupled to a single-mode fiber, in order to collapse its transverse spatial mode into a pure TEM_{00} ($\ell = 0$). After the fiber output, two wave plates compensated the polarization rotation introduced by the fiber (CP). To transform the polarization-entangled pairs into a hybrid-entangled state, photon B was sent through the quantum transferrer $\pi \rightarrow o_2$, which converted the polarization quantum states into the corresponding OAM states. After the transferrer operation the polarization-entangled state was transformed into the hybrid entangled state $\frac{1}{\sqrt{2}}(|H\rangle_\pi^A|+2\rangle_{o_2}^B - |V\rangle_\pi^A|-2\rangle_{o_2}^B)$. After the aperture F, the inverse $o_2 \rightarrow \pi$ transferrer and a polarization analysis set was used to analyze

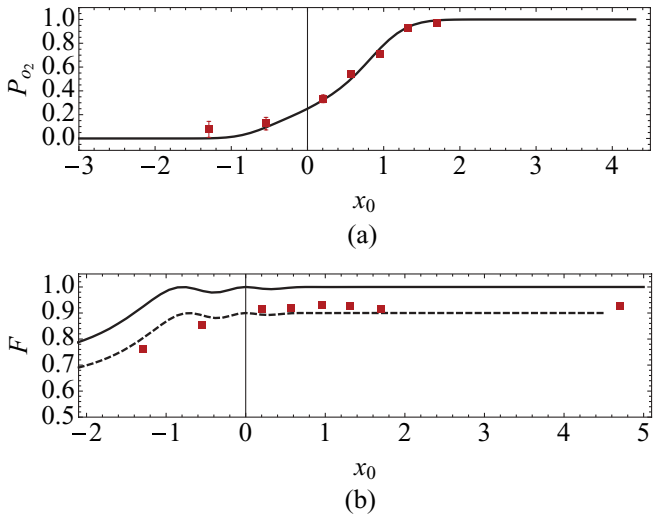

FIG. 9. (Color online) Information-preservation probability P_{o_2} (a) and fidelity (b) of the polarization-OAM hybrid-entangled pair of photons as a function of the planar aperture edge position x_0, given in units of the beam waist w_0: theoretical predictions (continuous line) and the one rescaled by the maximum value of measured fidelity (dashed line) compared to experimental data (squares).

the OAM photon state. Ultimately, the photon was coupled to a single-mode fiber and then detected by D_B, connected to the coincidence box (CB), which recorded the coincidence counts $\{D_A, D_B\}$.

The experimental results for the probability P_{o_2} and the fidelity F are shown in Fig. 9. We observed that the state fidelity achieves somewhat lower values than what was predicted (and than what was obtained for the classical experiment case), particularly when the aperture blocked more than half of the beam. It is clear from the figure that the fidelity reduction cannot be entirely ascribed to the aperture, as it remains constant even when the aperture is moved completely off the beam. The maximum fidelity of the two-photon state is presumably decreased by imperfections in the source, preparation, and measurement stages, to which it is typically more sensitive than in the single photon state. To account for this effect, we plotted the expected theoretical curves rescaled by the maximum value of measured fidelity. This rescaled curve exhibits a reasonable agreement with the experimental data [dashed line in Fig. 9(b)].

V. CONCLUSIONS

In this paper we tested the robustness of OAM-encoded qubits, which provide a useful and versatile quantum-communication resource. In the classical case, we first demonstrated that the information encoded in a bidimensional subspace of the OAM can be retrieved probabilistically in the same subspace even if the state is highly perturbed in such a way as to block a significant fraction of the transverse extension of the mode. The experimental results are in good agreement with the theoretical model.

We then proceeded to demonstrate also in the single-photon regime, by using polarization-OAM entangled photon pairs, the high resilience of single-photon bidimensional OAM states. We verified that hybrid entanglement correlations persist even in high-loss conditions.

ACKNOWLEDGMENTS

This work was supported by Project HYTEQ-FIRB, Finanziamento Ateneo 2009 of Sapienza Università di Roma, and European Project PHORBITECH of the FET Program (Grant No. 255914).

[1] M. A. Nielsen and I. L. Chuang, *Quantum Computation and Quantum Information* (Cambridge University Press, Cambridge, UK, 2000).
[2] N. Gisin, G. Ribordy, W. Tittel, and H. Zbinden, Rev. Mod. Phys. **74**, 145 (2002).
[3] J. L. O'Brien, Science **318**, 1567 (2007).
[4] E. Nagali, L. Sansoni, L. Marrucci, E. Santamato, and F. Sciarrino, Phys. Rev. A **81**, 052317 (2010).
[5] E. Nagali, D. Giovannini, L. Marrucci, S. Slussarenko, E. Santamato, and F. Sciarrino, Phys. Rev. Lett. **105**, 073602 (2010).
[6] A. Mair, V. Alipasha, G. Weihs, and A. Zeilinger, Nature (London) **412**, 313 (2001).
[7] G. Molina-Terriza, J. P. Torres, and L. Torner, Nat. Phys. **3**, 305 (2008).
[8] S. Franke-Arnold, L. Allen, and M. Padgett, Laser Photonics Rev. **2**, 299 (2008).
[9] E. Nagali *et al.*, Opt. Express **17**, 18745 (2009).
[10] E. Nagali, F. Sciarrino, F. De Martini, L. Marrucci, B. Piccirillo, E. Karimi, and E. Santamato, Phys. Rev. Lett. **103**, 013601 (2009).
[11] E. Nagali *et al.*, Nat. Photonics **3**, 720 (2009).
[12] L. Marrucci, C. Manzo, and D. Paparo, Phys. Rev. Lett. **96**, 163905 (2006).
[13] J. Arlt, J. Mod. Opt. **50**, 1573 (2003).
[14] G. Gibson *et al.*, Opt. Express **12**, 5448 (2004).
[15] M. V. Vasnetsov, V. A. Pas'ko, and M. S. Soskin, New J. Phys. **7**, 46 (2005).
[16] C. Paterson, Phys. Rev. Lett. **94**, 153901 (2005).
[17] C. Gopaul and R. Andrews, New J. Phys. **9**, 94 (2007).
[18] G. Gbur and R. K. Tyson, J. Opt. Soc. Am. A **25**, 225 (2008).
[19] B. J. Pors, C. H. Monken, E. R. Eliel, and J. P. Woerdman, Opt. Expr. **19**, 6671 (2011).
[20] G. A. Tyler and R. W. Boyd, Opt. Lett. **34**, 142 (2009).
[21] A. A. Semenov and W. Vogel, Phys. Rev. A **81**, 023835 (2010).
[22] E. Nagali and F. Sciarrino, Opt. Express **18**, 18243 (2010).

[23] E. Karimi, J. Leach, S. Slussarenko, B. Piccirillo, L. Marrucci, L. Chen, W. She, S. Franke-Arnold, M. J. Padgett, and E. Santamato, Phys. Rev. A **82**, 022115 (2010).
[24] M. J. Padgett and J. Courtial, Opt. Lett. **24**, 430 (1999).
[25] E. Karimi, B. Piccirillo, L. Marrucci, and E. Santamato, Opt. Lett. **34**, 1225 (2009).
[26] A. K. Jha, B. Jack, E. Yao, J. Leach, R. W. Boyd, G. S. Buller, S. M. Barnett, S. Franke-Arnold, and M. J. Padgett, Phys. Rev. A **78**, 043810 (2008).
[27] B. Jack *et al.*, New J. Phys. **11**, 103024 (2009).
[28] P. G. Kwiat, E. Waks, A. G. White, I. Appelbaum, and P. H. Eberhard, Phys. Rev. A **60**, R773 (1999).